Experimental and simulation investigation for rotor bar fault diagnosis in closed-loop induction motors drives

Seddik Tabet[1], Adel Ghoggal[1], Hubert Razik[2], Ishaq Amrani[1], Salah Eddine Zouzou[1]
[1]The Electrical Engineering Laboratory of Biskra LGEB, University of Biskra, Biskra, Algeria
[2]UMR Laboratory Ampère, University of Lyon, Lyon, France

Article Info

ABSTRACT

This research presents a comparative analysis of two broken rotor bar (BRB) fault identification techniques for closed-loop induction motors (IMs). Both motor current signal analysis and Hilbert transform (HT) rely on spectrum analysis by means of fast fourier transform (FFT). Both approaches have shown their ability to identify BRBs under varying loads. In contrast, the HT is deemed more efficient than the motor current signature analysis (MCSA) approach when the motor is working without load. To maintain a high-performance speed control and to compensate for BRBs effect on the mechanical speed, the approach of control used is direct torque control (DTC). Utilizing a real-time implementation in MATLAB/Simulink with the real-time interface (RTI) based on the dSPACE 1104 board, the efficacy of the two techniques was evaluated.

Corresponding Author:

Seddik Tabet
The Electrical Engineering Laboratory of Biskra LGEB, University of Biskra
07000 Biskra, Algeria
Email: seddik.thabet@univ-biskra.dz

1. INTRODUCTION

Due to their vast range of applications, induction motors (IMs) are among the most vital electrical equipment and efficiency in a variety of industrial applications, including pumps, compressors, fans, conveyors, and electric vehicles [1]. Furthermore, their utilization is in progress due to their low cost, ruggedness providing flexibility in a wide range of operating circumstances [2]. Besides that, the high reliability of IMs for ensuring an uninterrupted and problem-free functioning in the industry. IMs are subject to a variety of inevitable stressors, including mechanical, electrical, thermal, and environmental restrictions. This last constraint leads to many faults within the motors. In addition, the non-obvious of the faults in early stages produces a catastrophic motor failure. Therefore, the industry will suffer financial losses. To avoid this last, the early fault detection and diagnosis of IM components is required for offering the adequate warning of the coming failures [3]–[8]. One of the important failures is broken rotor bar (BRB) which represents 10% of induction motor faults. Detecting this fault under a closed loop control is a challenge for many researchers. Therefore, many control techniques have been used and applied, such as field oriented control (FOC), direct torque control (DTC) [9], [10].

In this research, DTC have been used as a control mechanism owing to its simple construction, rapid response, and excellent decoupling [11], [12]. The control settings and switching frequency of the DTC cause the presence of a high frequency component in the stator current spectrum of a DTC-fed squirrel cage induction motor (SCIM). In addition to the control structure, the sideband amplitude around the supply frequency of the phase current will be impacted [13]–[16].

In order to analyze the stator current spectrum tow techniques were applied, the first one is considered as motor current signature analysis (MCSA) most typical malfunction signature and the second is the Hilbert transform (HT). Both techniques are to be compared to show their efficiency. The spectral leakage it's one of limitation of fast fourier transform (FFT) because of the finite time window. Thus, a high frequency resolution and variety of side band frequencies are required. At the frequencies listed in [17], [18] additional components have been induced in the stator current:

$$f_b = (1 \pm 2Ks)f_s, K = 1,2,3 \dots \tag{1}$$

Where f_b is the frequency of bar fractures, f_s is the frequency of supply and s is the lapse (slip).

This paper deals with experimentally validation of BRB fault diagnosis within SCIM using MCSA and MCSA via HT. Where the HT is proposed to defeat the difficulties in MCSA particularly at very low slip and it provide against the low-level load condition a very low sensitivity [9], [19]. The HT method is dependent on the envelope analysis of each stator current for BRB [20]. In any case, the envelope was produced by modulation of the stator current. Both MCSA and MCSA through HT are simulated in closed loop with DTC control, and the results are shown to validate the efficacy and practicability of the HT method, which provides the ability to identify BRB faults even in no-load conditions, in comparison to MCSA.

2. METHOD

DTC is a control philosophy that makes advantage of AC machines' torque and flux-producing capabilities when supplied by a voltage source inverter without current regulator loops. However, it achieves the same performance as a vector control drive [21]. Figure 1 displays the DTC method for selecting the six non-zero and two zero voltage vectors of an inverter based on instantaneous torque and stator flux magnitude errors (Figure 2). This is accomplished by selecting the correct sector in the spatial vector modulation, which will be detailed in more detail later in this section. The DTC technique estimates magnetic flux and torque by measuring the motor's voltages and currents. If the torque or flux exceeds a certain tolerance range (hysteresis band), the variable speed drive transistors are changed to the next state in order to bring the torque or flux to inside the tolerance range as fast as possible [20], [22].
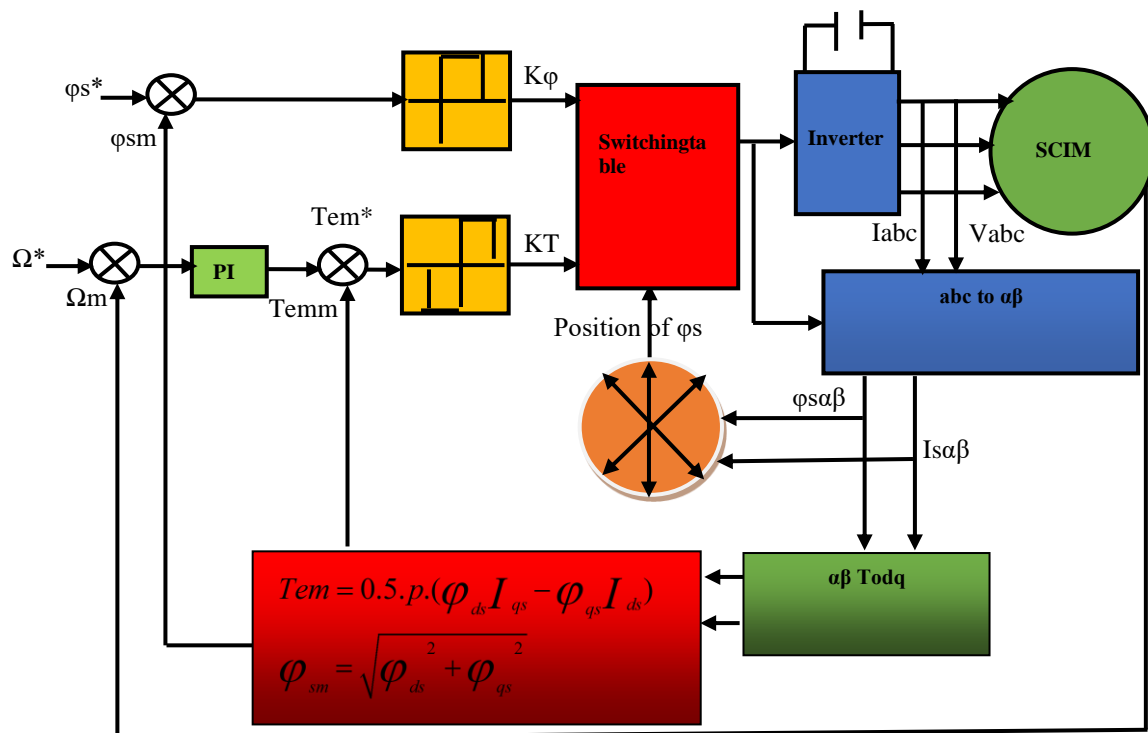

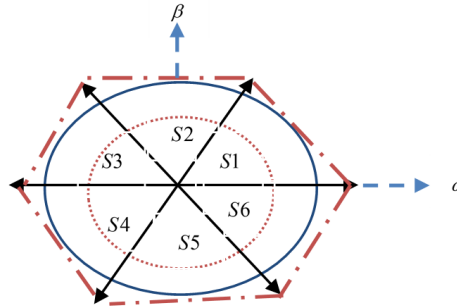Figure 1. Block diagram of DTC of the SCIM

Figure 2. Inverter output voltage sectors

2.1. Behavior of the stator flux

The following equation can be used to calculate the stator flux, in the (α, β) reference. Where: $\bar{\varphi}_S$ represent the stator flux vector; $\bar{R}_S$ represent the stator resistance; $\bar{V}_S$ represent the voltage vector.

$$\bar{V}_S = \bar{R}_S \bar{I}_S + \frac{d\bar{\varphi}_S}{dt} \tag{2}$$

2.2. Behavior of the torque

According to the following formula, electromagnetic torque is proportional to the vector product of stator and rotor flux [23].

$$Te = K(\bar{\varphi}_S \times \bar{\varphi}_r) = K|\varphi_S||\varphi_r|\sin(\sigma) \tag{3}$$

With: $\bar{\varphi}_S$ is the vector of stator flux; $\bar{\varphi}_r$ is the vector of rotor flux; σ is the angle between the vectors of stator and rotor flux.

2.3. Sequences of the switching table

The DTC algorithm (Figure 1) identifies the correct inverter voltage vector to be applied to the induction motor based on the hysteresis state of the torque, flux, and the switching sector of the stator flux, indicated by (α). The parameters of an inverter's switching device are the outputs of the switching vectors in the various stator flux sectors.

$$\alpha = \angle \bar{\varphi}_S = tan^{-1}(\frac{\varphi_{S\beta}}{\varphi_{S\alpha}}) \tag{4}$$

According to Table 1, the vectors of active switching are $\bar{V}_1$ through $\bar{V}_6$ as well as the zero switching vectors $\bar{V}_0$ and $\bar{V}_7$. The stator flux switching sectors may be organized according to the six sectors shown in Table 1.

$$\alpha = \begin{cases} -30^0 < \alpha_1 < 30^0 \\ 30^0 < \alpha_2 < 90^0 \\ 90^0 < \alpha_3 < 150^0 \\ 150^0 < \alpha_4 < 210^0 \\ 210^0 < \alpha_5 < 270^0 \\ 270 < \alpha_1 < 330^0 \end{cases} \tag{5}$$

Table 1. Sequences of inverter voltage vector switching

Sector	(S)	1	2	3	4	5	6
$K_\varphi = 1$	$K_T = 1$	110	010	011	001	101	100
	$K_T = 0$	111	000	111	000	111	000
	$K_T = -1$	101	100	110	010	011	001
$K_\varphi = 0$	$K_T = 1$	010	011	001	101	100	110
	$K_T = 0$	000	111	000	111	000	111
	$K_T = -1$	001	101	100	110	010	011

2.4. Hilbert transform for detection broken rotor bar fault

As is well known, HT has been used in a number of scientific fields, involving signal transmission, processing of geophysical data, and detection or diagnosis of faults [17]. In our example, HT is used to identify IMs with BRBs. This section discusses briefly the use of HT for stator current analysis of SCIM under a closed-loop drive [19], [24]. $\hat{\imath}_S(t)$ is the mathematical description of an actual signal's HT $i_S(t)$ [17]:

$$\hat{\imath}_S(t) = \frac{1}{\Pi} \int_{-\infty}^{+\infty} \frac{i_S(\tau)}{t-\tau} d\tau \tag{6}$$

The aforementioned analytical signal $\overline{\imath_S}(t)$ consists of connecting $i_S(t)$ and $\hat{\imath}_S(t)$:

$$\overline{\imath_S}(t) = i_S(t) + j\hat{\imath}_S(t) = a(t)e^{j\theta(t)} \tag{7}$$

Where:

$$a(t) = \sqrt{i_{Sa}^2(t) + \hat{\imath}_{Sa}^2(t)} \text{ and } \theta(t) = \tan^{-1}\theta\left(\frac{i_{Sa}(t)}{\hat{\imath}_{Sa}(t)}\right) \tag{8}$$

Where a(t) is the so-called envelope ($\overline{\imath}_{Sa}(t)$ instantaneous amplitude), which might represent how $i_{Sa}(t)$ energy changes in time, and $\theta(t)$ is the instantaneous phase of $\overline{\imath}_{Sa}(t)$. The processes for obtaining the diagnostic and analysis one-phase stator current envelope for the BRB scenario may be defined as [17]:
- Measure stator current on a single phase, indicated as $i_S(t)$.
- Calculate the HT of $i_S(t)$, also known as $\hat{\imath}_S(t)$ (in practice, the HT is calculated using an FFT based procedure [25]).
- Calculate the Hilbert modulus a(t) as shown in Figure 3 based on (21).
- Subtract the average of the dc component in a(t) and call the result $a(t)^*$, i.e $a(t)^* = a(t) - \text{mean}(a(t))$.
- Using FFT, extract the spectrum of $a(t)^*$ and study the BRB indication, i.e. the components in the spectrum at frequencies of 2sf1 and 4sf1.

As a result, the envelope can be used to identify a BRB fault. To identify BRBs faults in a particular the use of a FFT either the stator current's HT or its modulus and applying it to the diagnosis of asymmetric rotor defects, particularly under no-load situations, provides significant advantages [9], [19]. Aside from that, this study focuses on identifying rotor asymmetries in SCIM drives running at low loads and the resolution of difficulties caused by the switching closed-loop method when the SCIM is operating at high frequencies [13], [26], [27].
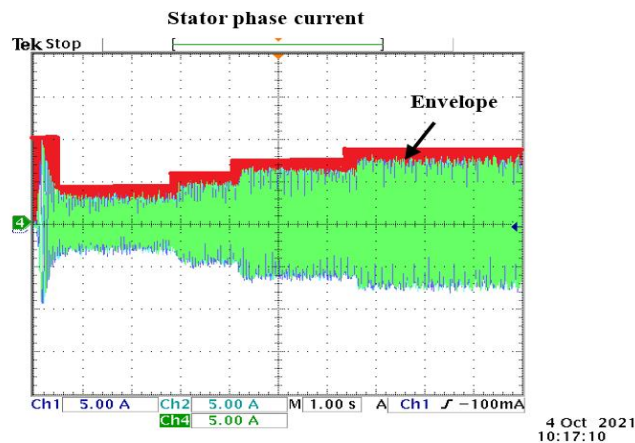

Figure 3. Stator current Ia and its envelope for two BRBs operating under distinct load conditions

3. RESULTS AND DISCUSSION

As indicated in Figure 4, the BRB fault was manufactured in experimental testing by drilling a 3 mm-diameter hole at each rotor bar depth. Figure 5 demonstrates the experimental configuration and software/hardware connection of the testing apparatus. Using a numerical oscilloscope equipped with a real-time interface (RTI) through a dSPACE 1104 board linked to a PC running control desk software, the results

are gathered. The following are the primary components of the testing apparatus, as seen in Figure 5: 1) three-phase 3-kW SCIM (see Table 2 for more details), 2) the SCIM is coupled with synchronous generator provide variable load torque, 3) the Semikron power converter is comprised of a rectifier and insulated gate bipolar transistors (IGBT) inverter with adaption interfaces (5–15 V), 4) incremental encoder that permits rotor speed measurement, 5) current and voltage sensors of the Hall type, 6) automatic transform (0–450 V), 7) dSpace 1,104 linked to a PC with control desk software, 8) mechanical coupling between SCIM and synchronous generator, 9) torque sensor, 10) variable load of the synchronous generator, 11) continuous feed, and 12) multimeter.

Figure 4. Induction motor rotor bar fracture (broken)
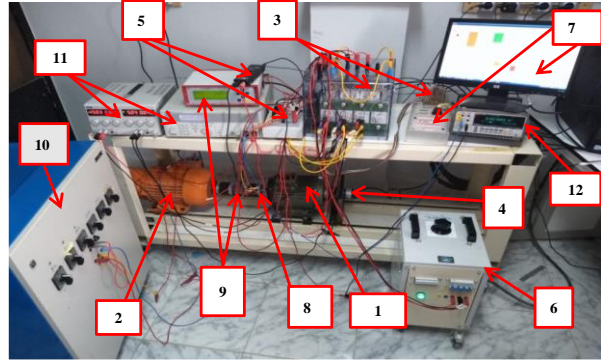
Figure 5. Photo of experimental setup and software/hardware linkage

The dS1104 accepts sensor input signals (speed, current) and produces digital control signals. These signals are delivered to a MATLAB/Simulink application using an RTI that provides input/output (I/O) ports for the dS1104 in Simulink's library. The implementation on the dS1104 board will change it into a hardware (dspace 1104) real-time system, as opposed to a software system (Simulink). Using control desk software, system variables such as gains, and reference signals. are modified to achieve the desired control behavior. The DC-bus converter is stabilized by filtering the input voltage using a three-phase rectifier. Analog control signals are sent through dspace and are shifted from one to the next (0-5 V). To activate the IGBTs of the inverter, however, the control signals are amplified to (0-15 V) using a laboratory-built adaptive amplifier. Lastly, the SCIM is used to control the inverter through the control desk. The experimental outcomes are shown using an oscilloscope connected to RTI.

Table 2. Technical data of SCIM

Parameter	Value
Rated power	3 kW
Rated voltage	380 V
Rated frequency	50 Hz
Stator winding connection	Y
Pole pairs number	2
Rotor slot number	28
Stator slots number	36
Air-gap length	0.3 mm
Rotor inertia moment	0.023976- Kg. m^2
Stator winding turns per coil	25
Stator per phase resistance	1.8 Ω
Rotor bar resistance	0.02856 mΩ
End ring resistance	0.01856 mΩ
Stator per phase leakage inductance	10 mH
End ring leakage inductance	0.04535 μH
Rotor bar leakage inductance	1.27 μH
Stator phase 'a' winding scheme	A-0-9'-1-10'-2-11'-18-27'-19-28'-20-29'-X

3.1. Healthy state of the squirrel cage induction motor

Figure 6 depicts the DTC SCIM's healthy testing results. In 10 seconds, several mechanical and electrical parameters are measured. As seen in Figure 6(a), the rotor speed response is given without overrun (1 div=200 rpm). The rotor speed looks to be a useful reference point. As shown in figure, the growth of the

stator flux components (1 div=0.5 Wb) in the plane (α,β) is exactly circular as showed in Figure 6(e). The electromagnetic torque (1 div=10 Nm) in Figure 6(b) is dynamically rapid. Where the wave patterns of phase currents in the stator (1 div=5 A) are mostly sinusoidal with variable amplitudes according to the fluctuating load, as seen in Figures 6(f) and the zoom of stator current in Figure 6(g). As shown in Figures 6(c) the functioning of the machine in reverse rotation at high speed (1 div=500 rpm), and Figure 6(d) at low speed (1 div=200 rpm) indicates the DTC superior performance.

(a)   (b)   (c)

(d)   (e)   (f)

(g)
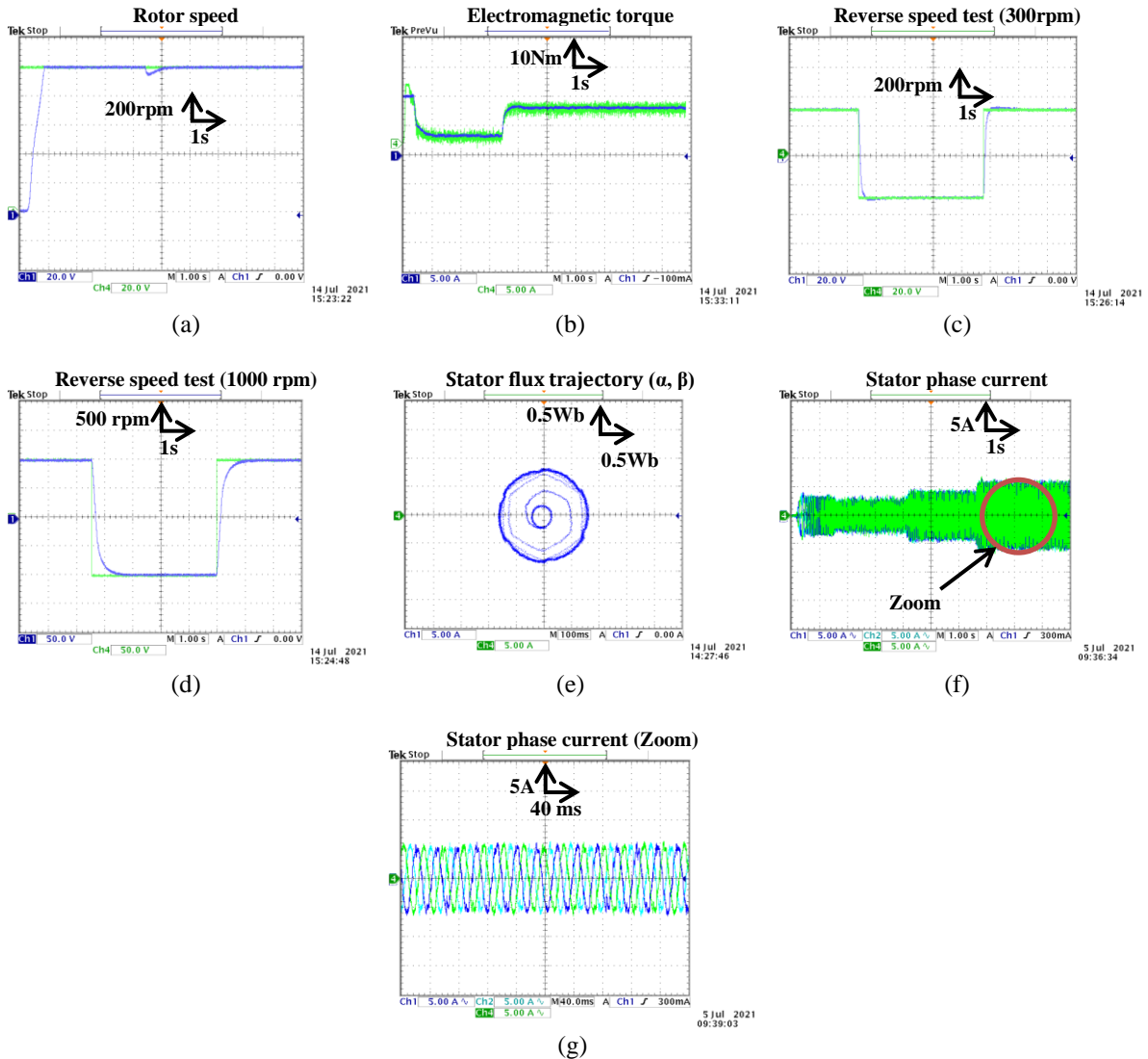
Figure 6. In a healthy condition, the mechanical and electrical quantities of the DTC (a) rotor speed, (b) electromagnetic torque, (c) reverse speed test (300 rpm), (d) reverse speed test (1,000 rpm), (e) stators flux trajectory (α, β), (f) stators phase current, and (g) stators phase current (zoom)

3.2. One broken rotor bar fault of the squirrel cage induction motor

One cracked rotor bar was found during testing of the motor. Based on the study of the findings acquired from one BRB Figure 7 compared to the healthy condition Figure 6 demonstrates that the rotor speed is unaffected by a single BRB owing to closed-loop regulation, as seen in Figure 7(a). The default value affects the electromagnetic torque. By the emergence of distinct waves when a weight is applied, as seen in the Figure 7(b). In Figures 7(f) the amplitude of oscillating stator phase current is greater than in a healthy condition and the Figure 7(g) as well as. The flux trajectory of the stator is unaffected, as seen in Figure 7(e). Figures 7(c) illustrate the excellent performance of the DTC during reverse speed operating at low speed (1 div=200 rpm) and Figure 7(d) at high speed (1 div=500 rpm).
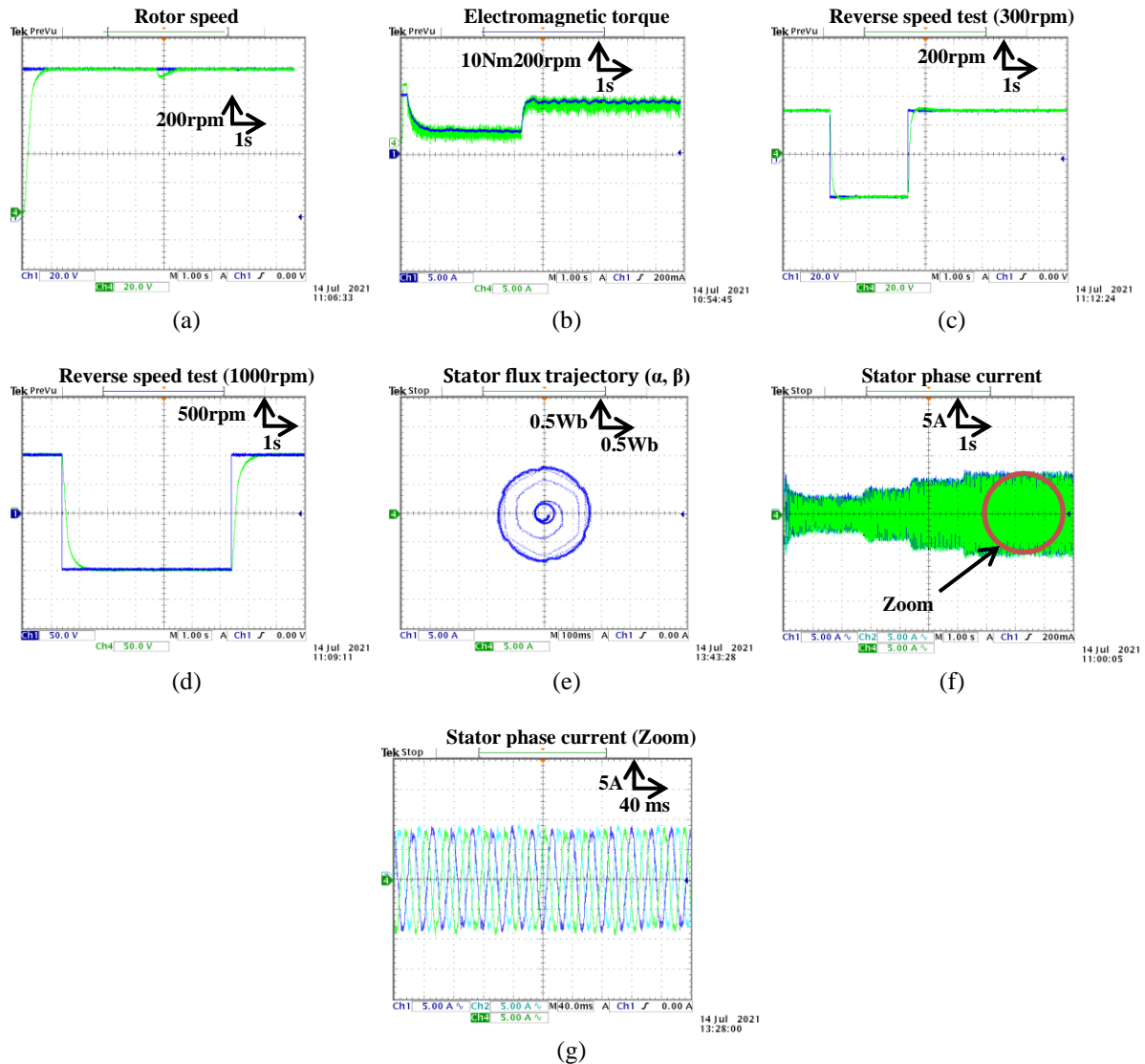
Figure 7. Mechanical and electrical DTC faulty values indicate one damaged rotor bar: (a) rotor speed, (b) electromagnetic torque, (c) reverse speed test (300 rpm), (d) reverse speed test (1,000 rpm), (e) stator flux trajectory (α, β), (f) stator phase current, and (g) stator phase current (zoom)

The speed of rotation of the SCIM operating under the DTC technique is 1,000 rpm (Figure 6), and frequency fundamental related to rotational speed under no-load circumstances in a healthy case is 33,64 Hz (Figure 8(a)). Figures 8 and 9 display the FFT's results in the form of normalized spectra. This last image displays phase current's FFT (MCSA) and the filtered phase current envelope $i_{env}(t)$, respectively. Figure 8 shows the results of the stator phase current processing. As demonstrated in Figures 8(a) and (b) for the healthy and BRB situations, respectively, at no-load, the frequency components of the BRB state are obscured by the mains frequency component spectral leakage. Figures 8(c)-(e), under 25%, 50%, and 75% load conditions, respectively, clearly illustrate the frequency characteristic components of the BRB as the load increases. The fault harmonic component $(1 \pm 2s)f_s(Hz)$ evident on the low, medal, and full load spectrometers. However, the amplitude of the harmonics increases as the load increases from 25% to 75%. As illustrated in Table 3 and Figure 8, Under no-load or even low-load conditions, the typical MCSA approach is unable of detecting a BRB problem. Alternatively, this approach is effective in detecting rotor asymmetries at high loads.

The HT is based on an analysis of the positive peaks in the oscillations of the stator phase current (envelope). Figure 9 shows the results of the identified envelope processing. Figure 9(a) depicts healthy instances. Compared to Figure 8(b) under no load, Figure 9(b) clearly displays the frequency characteristic components associated with a BRB failure. The fault harmonic component $2sf_s(Hz)$ and $4sf_s(Hz)$ as seen in

the Figures 9(b)-(e), are plainly evident on the no-load, low, medal, and 75% load specters. In contrast, the amplitude of the harmonic increases from no-load to 75% load. The HT can conclusively detect the frequency signature associated with a BRB failure under any load scenario, even complete no-load.
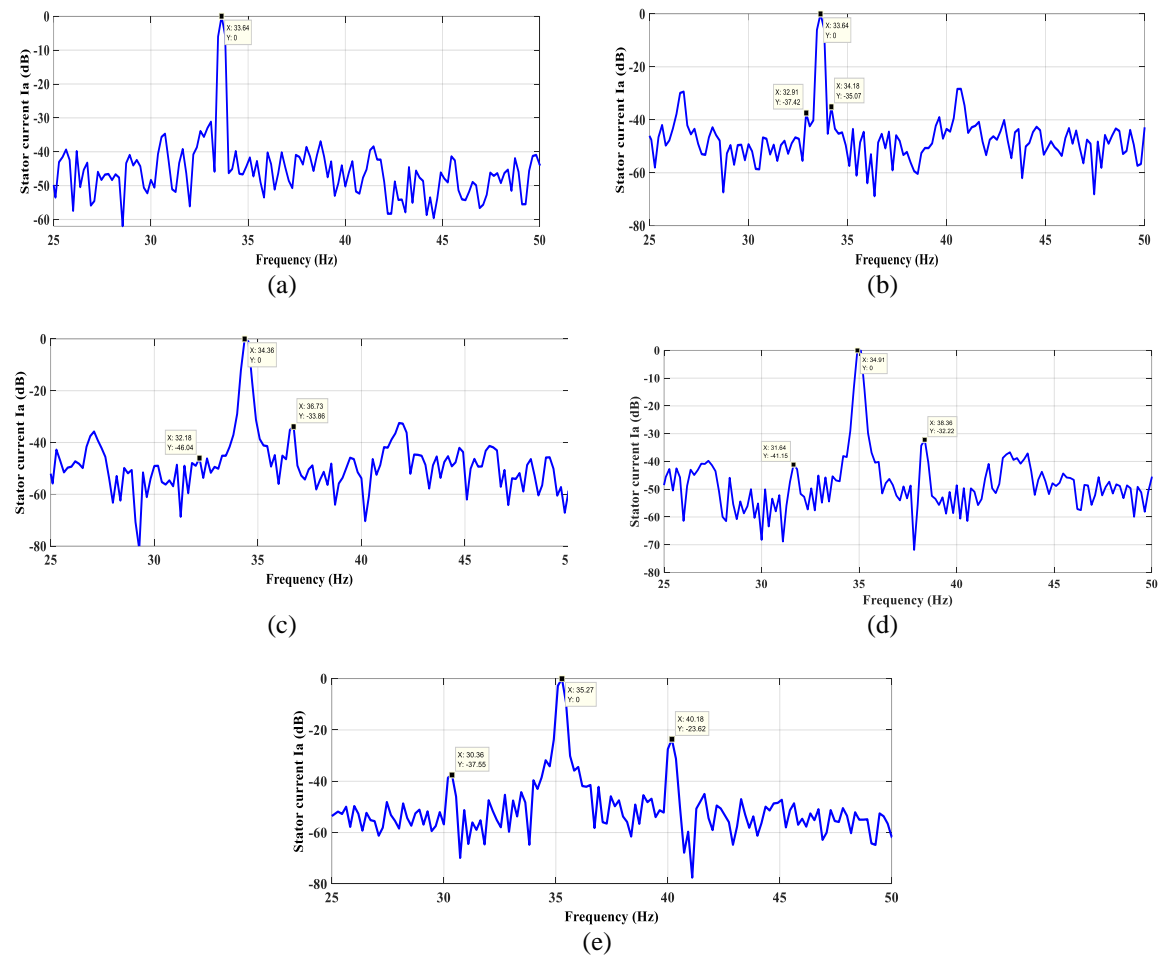

Figure 8. The current phase spectrum under a DTC strategy (a) healthy motor, (b) one BRB at no-load condition, (c) one BRB at 25% load condition, (d) one BRB at 50% load condition, and (e) one BRB at 75% load condition

Table 3. Experimental examinations of a healthy and defective motor using the DTC approach

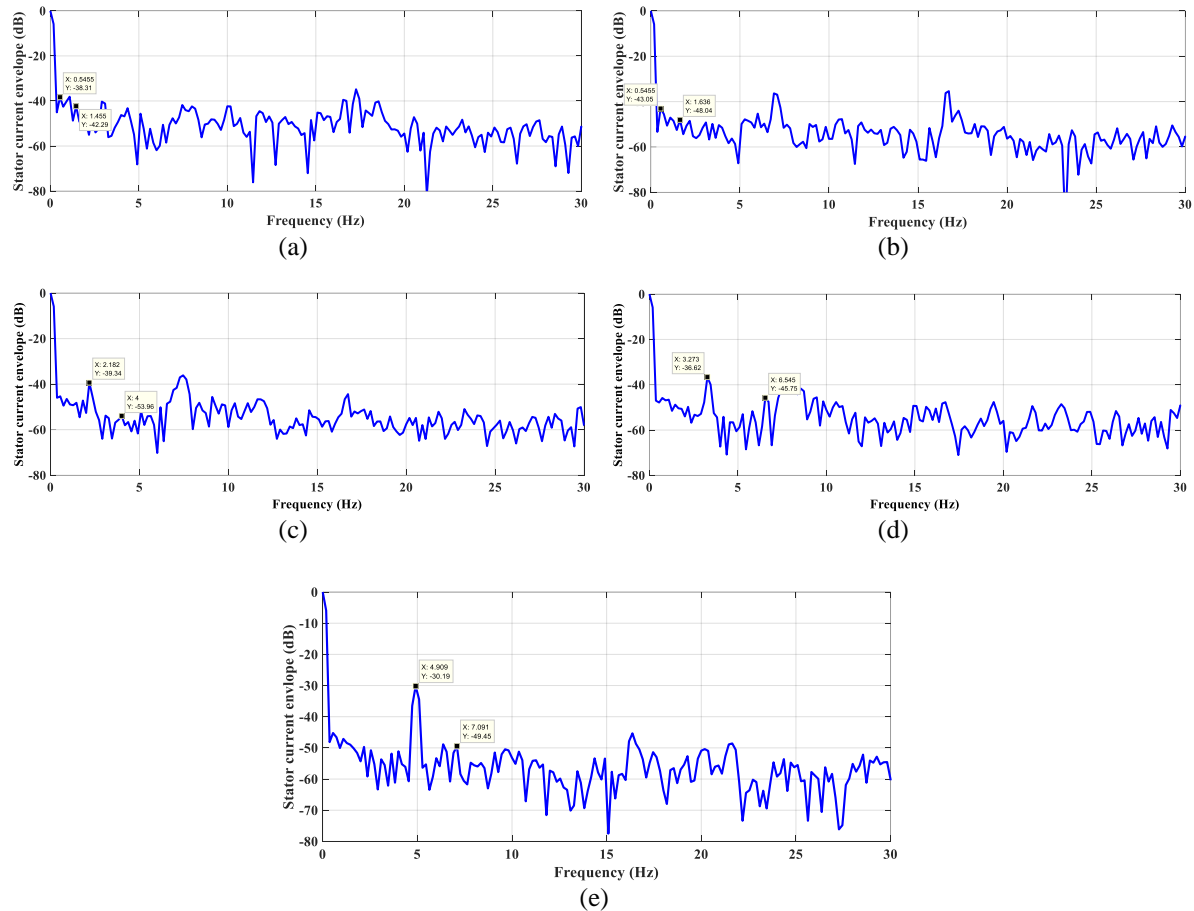| Motor	Load	Slip (%)	$2sf_s(Hz)$	$4sf_s(Hz)$	$(1 \pm 2s)f_s(Hz)$
Healthy	No load	0.009	0.54	1.45	-
One BRB	No load	0.009	0.54	1.63	34.18
					32.91
	25% load	0.029	2.18	4	36.73
					32.18
	50% load	0.045	3.27	7.09	38.36
					31.64
	75% load	0.05	4.9	7.63	40.18
					30.36
Two BRB	No load	0.009	0.54	1.27	34.91
					32.18
	25% load	0.045	2.909	6	40.73
					28.91
	50% load	0.069	4.9	10	44.55
					24.73
	75% load	0.105	7.63	15.45	52
					21.45

Figure 9. The spectrum of the envelope of phase current using a DTC strategy: (a) healthy motor, (b) one BRB at no-load, (c) one BRB at 25%, (d) one BRB at 50% load, and (e) one BRB at 75% load

The study of Table 4 reveals that the computed frequencies in experimental data are very close to the inferred frequencies, and the errors are insignificant. The computed frequencies of the broken bar are 34.25 and 33.03 Hz, compared to 34.18 and 32.91 Hz that were determined. We identify very little flaws that might be overlooked.

Table 4. Magnitude and frequency of the spectrum and envelope of the stator current Ia

S=0.009	Experimental results			
	$(1+2s)f_s(Hz)$	$(1-2s)f_s(Hz)$	$2sf_s(Hz)$	$4sf_s(Hz)$
$f_{calculated}(Hz)$	34.25	33.03	0.61	1.22
$f_{deduced}(Hz)$	34.18	32.91	0.54	1.63
Magnitude (Hz)	-35.07	-37.42	-43.05	-48.04

4.   CONCLUSION

This study gives a simulation and experimental analysis of broken rotor fault using FFT analysis for electrical values based on stator phase current and its envelope for the SCIM under closed-loop driving. Using the MCSA and HT methods, a rotor fault signature was created. The machine's DTC mechanism. The outcomes demonstrate a good control dynamic in both healthy and defective machine instances. The MCSA approach was unable to identify the BRB issue in the absence of load. The basic frequency spectrum leaking conceals the fault frequency characteristic components. In contrast to the HT approach, this technique has shown its ability reliably detect BRB frequency characteristic components under any load condition, including absolute no-load, using just a single stator phase current and a minimal storage capacity. Because of these benefits, it is suitable for both software and hardware implementations. The experimental implementation validates the simulation tests and yields identical rotor failure signatures.

REFERENCES

[1] V. Biot-Monterde, A. Navarro-Navarro, I. Zamudio-Ramirez, J. A. Antonino-Daviu, and R. A. Osornio-Rios, "Automatic classification of rotor faults in soft-started induction motors, based on persistence spectrum and convolutional neural network applied to stray-flux signals," *Sensors*, vol. 23, no. 1, pp. 1–29, Dec. 2022, doi: 10.3390/s23010316.

[2] M. Tran *et al.*, "Robust fault recognition and correction scheme for induction motors using an effective IoT with deep learning approach," *Measurement*, vol. 207, p. 112398, Feb. 2023, doi: 10.1016/j.measurement.2022.112398.

[3] R. S. Kumar *et al.*, "A combined HT and ANN based early broken bar fault diagnosis approach for IFOC fed induction motor drive," *Alexandria Engineering Journal*, vol. 66, pp. 15–30, Mar. 2023, doi: 10.1016/j.aej.2022.12.010.

[4] A. Boushaba, S. Cauet, A. Chamroo, E. Etien, and L. Rambault, "Comparative study between physics-informed CNN and PCA in induction motor broken bars MCSA detection," *Sensors*, vol. 22, no. 23, pp. 1–17, Dec. 2022, doi: 10.3390/s22239494.

[5] D. Liu, H. Inoue, and M. Kanemaru, "Robust motor current signature analysis (MCSA)-based fault detection under varying operating conditions," in *2022 25th International Conference on Electrical Machines and Systems (ICEMS)*, Nov. 2022, pp. 1–5, doi: 10.1109/ICEMS56177.2022.9983454.

[6] K. M. Siddiqui, K. Sahay, and V. K. Giri, "Health monitoring and fault diagnosis in induction motor-a review," *International Journal of Advanced Research in Electrical, Electronics and Instrumentation Engineering*, vol. 3, no. 1, pp. 6549–6565, 2014.

[7] R. Tiwari, *Rotor systems: analysis and identification*. Boca Raton: CRC Press, 2017, doi: 10.1201/9781315230962.

[8] G. H. Bazan, P. R. Scalassara, W. Endo, A. Goedtel, R. H. C. Palacios, and W. F. Godoy, "Stator short-circuit diagnosis in induction motors using mutual information and intelligent systems," *IEEE Transactions on Industrial Electronics*, vol. 66, no. 4, pp. 3237–3246, Apr. 2019, doi: 10.1109/TIE.2018.2840983.

[9] M. Abd-el-Malek, A. K. Abdelsalam, and O. E. Hassan, "Induction motor broken rotor bar fault location detection through envelope analysis of start-up current using Hilbert transform," *Mechanical Systems and Signal Processing*, vol. 93, pp. 332–350, Sep. 2017, doi: 10.1016/j.ymssp.2017.02.014.

[10] Y. Gritli, A. O. di Tommaso, R. Miceli, F. Filippetti, and C. Rossi, "Closed-loop bandwidth impact on MVSA for rotor broken bar diagnosis in IRFOC double squirrel cage induction motor drives," in *2013 International Conference on Clean Electrical Power (ICCEP)*, Jun. 2013, pp. 529–534, doi: 10.1109/ICCEP.2013.6586904.

[11] G. Ozkurt and E. Zerdali, "Design and implementation of hybrid adaptive extended Kalman filter for state estimation of induction motor," *IEEE Transactions on Instrumentation and Measurement*, vol. 71, pp. 1–12, 2022, doi: 10.1109/TIM.2022.3144729.

[12] S. el Daoudi, L. Lazrak, N. el Ouanjli, and M. A. Lafkih, "Sensorless fuzzy direct torque control of induction motor with sliding mode speed controller," *Computers & Electrical Engineering*, vol. 96, p. 107490, Dec. 2021, doi: 10.1016/j.compeleceng.2021.107490.

[13] A. M. da Silva, R. J. Povinelli, and N. A. O. Demerdash, "Induction machine broken bar and stator short-circuit fault diagnostics based on three-phase stator current envelopes," *IEEE Transactions on Industrial Electronics*, vol. 55, no. 3, pp. 1310–1318, Mar. 2008, doi: 10.1109/TIE.2007.909060.

[14] A. Bellini, C. Concari, G. Franceschini, and C. Tassoni, "Different procedures for the diagnosis of rotor fault in closed loop induction motors drives," in *2007 IEEE International Electric Machines & Drives Conference*, May 2007, pp. 1427–1433, doi: 10.1109/IEMDC.2007.383638.

[15] Y. Zhongming and W. Bin, "A review on induction motor online fault diagnosis," in *Proceedings IPEMC 2000. Third International Power Electronics and Motion Control Conference (IEEE Cat. No.00EX435)*, 2000, pp. 1353–1358, doi: 10.1109/IPEMC.2000.883050.

[16] S. Nandi, H. A. Toliyat, and X. Li, "Condition monitoring and fault diagnosis of electrical motors - a review," *IEEE Transactions on Energy Conversion*, vol. 20, no. 4, pp. 719–729, Dec. 2005, doi: 10.1109/TEC.2005.847955.

[17] R. Puche-Panadero, M. Pineda-Sanchez, M. Riera-Guasp, J. Roger-Folch, E. Hurtado-Perez, and J. Perez-Cruz, "Improved resolution of the MCSA method via Hilbert transform, enabling the diagnosis of rotor asymmetries at very low slip," *IEEE Transactions on Energy Conversion*, vol. 24, no. 1, pp. 52–59, Mar. 2009, doi: 10.1109/TEC.2008.2003207.

[18] W. Dehina, M. Boumehraz, and F. Kratz, "On-line detection and estimation of harmonics components in induction motors rotor fault through a modified Prony's method," *International Transactions on Electrical Energy Systems*, vol. 31, no. 2, pp. 1–16, Feb. 2021, doi: 10.1002/2050-7038.12737.

[19] B. Xu, L. Sun, L. Xu, and G. Xu, "Improvement of the Hilbert method via ESPRIT for detecting rotor fault in induction motors at low slip," *IEEE Transactions on Energy Conversion*, vol. 28, no. 1, pp. 225–233, Mar. 2013, doi: 10.1109/TEC.2012.2236557.

[20] A. Ammar, A. Benakcha, and A. Bourek, "Closed loop torque SVM-DTC based on robust super twisting speed controller for induction motor drive with efficiency optimization," *International Journal of Hydrogen Energy*, vol. 42, no. 28, pp. 17940–17952, Jul. 2017, doi: 10.1016/j.ijhydene.2017.04.034.

[21] A. Chikhi, M. Djarallah, and K. Chikhi, "A comparative study of field-oriented control and direct-torque control of induction motors using an adaptive flux observer," *Serbian Journal of Electrical Engineering*, vol. 7, no. 1, pp. 41–55, 2010, doi: 10.2298/SJEE1001041C.

[22] A. Ammar, A. Bourek, and A. Benakcha, "Nonlinear SVM-DTC for induction motor drive using input-output feedback linearization and high order sliding mode control," *ISA Transactions*, vol. 67, pp. 428–442, Mar. 2017, doi: 10.1016/j.isatra.2017.01.010.

[23] F. Khoucha, K. Marouani, K. Aliouane, and A. Kheloui, "Experimental performance analysis of adaptive flux and speed observers for direct torque control of sensorless induction motor drives," in *2004 IEEE 35th Annual Power Electronics Specialists Conference (IEEE Cat. No.04CH37551)*, 2004, pp. 2678–2683, doi: 10.1109/PESC.2004.1355255.

[24] B. Bessam, A. Menacer, M. Boumehraz, and H. Cherif, "Detection of broken rotor bar faults in induction motor at low load using neural network," *ISA Transactions*, vol. 64, pp. 241–246, Sep. 2016, doi: 10.1016/j.isatra.2016.06.004.

[25] L. Marple, "Computing the discrete-time 'analytic' signal via FFT," *IEEE Transactions on Signal Processing*, vol. 47, no. 9, pp. 2600–2603, 1999, doi: 10.1109/78.782222.

[26] M. Drif and A. J. M. Cardoso, "Stator fault diagnostics in squirrel cage three-phase induction motor drives using the instantaneous active and reactive power signature analyses," *IEEE Transactions on Industrial Informatics*, vol. 10, no. 2, pp. 1348–1360, May 2014, doi: 10.1109/TII.2014.2307013.

[27] L. Salah, G. Adel, K. Khaled, and B. Ahmed, "A comparative investigation between the mcsa method and the hilbert transform

for broken rotor bar fault diagnostics, in a closed-loop three-phase induction motor," *UPB Scientific Bulletin, Series C: Electrical Engineering and Computer Science*, vol. 81, no. 3, pp. 209–226, 2019, doi: 10.1019/UPB-sci_209-2268132019.

BIOGRAPHIES OF AUTHORS
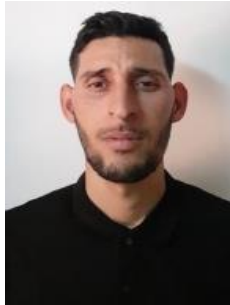
Seddik Tabet was born in Biskra, Algeria, in 1994. He received the master diploma in electrical engineering from the University of Biskra, in 2017. Mr. Tabet is a Ph.D. student with the University of Biskra and he is a member in the LGEB Laboratory. His focused on electrical machines and fault diagnosis in power electronics systemes and AC machines. He can be contacted at email: seddik.thabet@univ-biskra.dz.

Adel Ghoggal was born in Biskra, Algeria, in 1971. He received the Engineer and Magister diploma and the Ph.D. degree in electrical engineering from the University of Biskra, in 1996, 2005 and 2010 respectively. Mr. Ghoggal is an assistant professor with the University of Biskra since 2005 and he is a member in the LGEB Laboratory. His research interests are focused on electrical machines design and fault diagnosis in power electronics systems and AC machines. He can be contacted at email: ghoetudes@yahoo.fr.

Hubert Razik received the engineering degree from the Ecole Normale Supérieure, Cachan, France, in 1987, the Ph.D. degree in electrical engineering from the InstitutPolytechnique de Lorraine, Nancy, France, in 1991, and the Habilitation to Supervise Researchers from the Université Henri Poincaré, Nancy, in 2000. He is currently a Full Professor of electrical engineering with the Université Claude Bernard Lyon I, Villeurbanne, France. From 2016 to 2020, he is a Deputy Director of the Laboratory AMPERE-UMR 5005 (*www.ampere-lab.fr*), Villeurbanne, France. He has also been the Co-ordinator of the Master E-EE-A (Electronic, Electrical Energy, Automatic) of the University Claude Bernard Lyon 1 from 2016 to 2020. Since 2020, he is a 1,000 Talent Expert at the Shanghai Maritime University, Shanghai, China. His research interests include modeling, control, and monitoring conditions. He can be contacted at email: hubert.razik@univ-lyon1.fr.

Ishaq Amrani received the B.Sc. degree in electrical engineering from Oum-Elbouaghi University, Algeria in 2011, a M.Sc. degree in 2013. And doctorate degree in 2018 in energetic system control. Since 2018 he works as assistant professor at Biskra University. His research interests are in design and modeling of electromagnetic micro-actuators and micro-pumps. He can be contacted at email: ishaq.amrani@univ-biskra.dz.

Salah Eddine Zouzou was born in Biskra, Algeria, in 1963. He received his B.Sc. from National Polytechnic School, Algiers, in 1987, and his M.Sc. and Ph.D. from National Polytechnic Academy of Grenoble, France, in 1988 and 1991, respectively. He has authored or co-authored more than 50 scientific papers in national and international conferences and journals. He is a professor at the Electrical Engineering Department, Biskra University, and he has been the director of the electrical engineering laboratory of Biskra since 2004. His research interests are focused on the design and condition monitoring of AC motors. He can be contacted at email: zouzou_s@hotmail.com.